AIMS Mathematics, 9(6): 15097–15118.
DOI: 10.3934/math.2024732
Received: 20 February 2024
Revised: 23 March 2024
Accepted: 19 April 2024
Published: 26 April 2024

https://www.aimspress.com/journal/Math

Research article

Analytical and numerical investigation of viscous fluid-filled spherical slip cavity in a spherical micropolar droplet

Abdulaziz H. Alharbi[1,*] **and Ahmed G. Salem**[2,*]

[1] Department of Mathematics, Jamoum University College, Umm Al-Qura University, Jamoum, 25375, Makkah, Saudi Arabia

[2] Department of Mathematics, Faculty of Science, Mansoura University, 35516, Mansoura, Egypt

* **Correspondence:** Email: ahhrbe@uqu.edu.sa, a.g.salem@mans.edu.eg.

Abstract: This article presents an analytical and numerical investigation on the quasi-steady, slow flow generated by the movement of a micropolar fluid drop sphere of at a concentrical position within another immiscible viscous fluid inside a spherical slip cavity. Additionally, the effect of a cavity with slip friction along with the change in the micropolarity parameter on the movement of the fluid sphere is introduced. When Reynolds numbers are low, the droplet moves along a diameter that connects their centres. The governing and constitutive differential equations are reduced to a computationally convenient form using appropriate transformations. By using the resulting linear partial differential equations for the stream functions and using the method of separation variables, we can obtain their solutions. General solutions for velocity fields are found using spherical coordinate systems, which are based on the concentric point of the cavity; this allows to obtain solutions to the Navier-Stokes equations internal and external to the spherical droplet. The vorticity-microrotation boundary condition is used in regard to the micropolar droplet case in a viscous fluid. The normalised drag forces acted upon the micropolar drop are illustrated via graphs and tables for diverse values of the viscosity ratio and drop-to-wall radius ratio, with the change of the spin parameter that attaches the microrotation to vorticity. The correction wall factor is shown to increase with an increase in the drop-to-wall radius ratio, when moving from the gas bubble case to the solid sphere case, with an increase in the micropolarity parameter, and with an increase in the slip frictional resistance. This study is relevant due to its potential uses in a variety of biological, natural, and industrial processes, including the creation of raindrops, the investigation of blood flow, fluid-fluid extraction, the forecasting of weather conditions, the rheology of emulsions, and sedimentation phenomena.

Keywords: low Reynolds numbers; micropolar fluid; vorticity-microrotation condition; spherical slip cavity
Mathematics Subject Classification: 35Q30, 76B99, 76D05, 76T06

Nomenclature

$\vec{u}$	the fluid velocity vector (m/s)
p	the fluid pressure at any point ($Kg.m\,s^{-2}$)
$\mathbf{m}$	the couple stress tensor
$\mathbf{I}$	the unit dyadic
$\vec{w}$	the fluid vorticity vector
E^2	the axially symmetric Stokesian operator
$I_n(\cdot)$	the modified Bessel function of order, n, of the first kind
$K_n(\cdot)$	the modified Bessel function of order, n, of the second kind
$G_n(\cdot)$	the Gegenbauer polynomial of the first kind of order, n, and degree $-\frac{1}{2}$
a	radius of the spherical drop
b	radius of the spherical cavity
$t_{r\theta}^{(1)}$	the tangential stress component for micropolar flow
$t_{r\theta}^{(2)}$	the tangential stress component for viscous flow
A, B, C, D, E, M, N	unknowns in the system of the equations (4.20) - (4.26)
$\hat{A}, \hat{B}, \hat{C}, \hat{D}, \hat{E}, \hat{M}, \hat{N}$	unknowns in the system of the equations (5.2) - (5.8)
W	the correction wall factor for the slip cavity case
$\hat{W}$	the correction wall factor for the no-slip cavity case
Greek Letters	
$\mathbf{\Pi}$	the stress tensor ($Kg.m\,s^{-2}$)
$\vec{v}$	the fluid micro-rotation vector (s^{-1})
$\boldsymbol{\varepsilon}$	the alternating tensor
k	the micropolar vortex viscosity coefficient ($Kg.m^{-1}\,s^{-1}$)
(α, β, γ)	the micropolar gyro-viscosity coefficients ($Kg.m\,s^{-1}$)
(r, θ, ϕ)	the spherical coordinate systems
$(\vec{e}_r, \vec{e}_\theta, \vec{e}_\phi)$	the unit vectors
$\psi^{(1)}$	the stream function for the viscous flow in the cavity and out the drop
$\psi^{(2)}$	the stream function of the micropolar flow in the drop
μ_1	the viscous fluid's viscosity coefficient
μ_2	the micropolar fluid's viscosity coefficient
η	the slip frictional resistance coefficient for velocity vector

1. Introduction

Nature is abundant in drops and bubbles. Physically, these fluid particles may, in almost every circumstance, be found in a continuum of other fluids and have a critical impact on the system's behaviour. Natural cloud formations made up of little water droplets are what trigger rainfall. Additionally, bubbles and drops frequently appear in industrial systems as transporters of both products and reactants, as well as in various chemical processes [1]. On the other hand, fluids employed in cooling or heating processes are mentioned as heat transfer fluids, which appear in industrial applications such as stream generators, die temperature controls, printing, presses, synthesis, extrusion, and catalysis [2–4]. Mass and heat transfer for the flow of Maxwell and Williams nanofluids are

discussed by [5, 6].

Stokes [7] introduced the earliest study on low Reynolds numbers, discussing the movement of a rigid sphere in viscous fluid phase. One significant parameter assessed was the force exerted by the surrounding fluid on the sphere. Stokes' solution led the study of the movement of particles with different shapes and fluid spheres. After Stokes, Rybczynski [8] and, independently, Hadamard [9], made traditional advancements in solving the steady, slow movement of the fluid sphere. They found that the drag force acted on the nondeformable fluid sphere by the surrounding fluid phase, based on the notion that, at the interface, both the velocity and tangential stress components were continuous. The extension of the works of Rybcznski [8] and Hadamard [9] to fluids with a micropolar microstructure was studied by both Kaloni and Niefer [10]. At the drop surface, the interface tensions tend to deform it. For instance, Taylor and Andreas [11] discussed the distortion of a droplet's spherical shape.

Since drops do not exist in isolation under low Reynolds numbers, it is essential to find out if the presence of adjacent nondeformable drops and/or their boundaries notably affect a droplet's navigation. These interplayed dynamics of drop behaviour have been studied extensively by exact, asymptotic, and numerical methods [12–26]. In [27], the behaviour of raindrops, water, and oil slicks was represented by a study model, characterized by linked spherical pores comprising an oil-containing formation rock. Rehman et al. [28] studied the fluid flow inside an extending cylindrical surface without any slip condition, with the relative velocity of the particles in the cylindrical surface and the Carreau fluid equal to zero. Asghar et al. [29] studied non-Newtonian fluid flow in a micro-channel passage in response to peristalsis under magnetic and electric fields. Additionally, a drop moving in a viscous/micropolar fluid along the midline of an impermeable tube results in a quasi-steady flow, as stated by Salem et al. [30].

The of Navier-Stokes equations presume that an internal structure is absent from fluid particles. In reality, fluid particles may exhibit many microscopic behaviours, such as protraction, constriction, or turnover, as in turbulent blood flow or polymer solutions, for instance. As a result, internal structure of fluid particles must be considered, specially when particles within the fluid can take on different forms. The micropolar fluid theory, initiated by Eringen [31–33], is an extensively recognised classical theory that considers such inner microstructure. According to this theory, particles can rotate and move independently from the general rotation and mobility of the fluid. Because of recent concerns, there is a new variable symbolising the fluid particles' angular velocity; hence, the classical model needs to include a new equation controlling that variable. Ferrofluids [34] are regarded as a micropolar phase, as they consist of Brownian magnetic particles in a colloidal fluid that have stabilised within a non-magnetic liquid host. Additionally, the granular flow can be regarded as a micropolar flow due to its rotation and particle microstructure. According to Hayakawa [35], the theoretical research on certain boundary value problems is consistent with pertinent experimental findings about granular flows. Recently, Walelign [36] used a mathematical model to study the effects of several thermo-physical influences on the transport rates of micropolar nanofluids near an inclined, exponentially stretched surface.

Early on in the development of fluid dynamics, it was common to apply the no-slip condition. Hence, for fluid flow, the Navier-Stokes equations were usually applied. As a result, the experimental observations appeared to confirm the validity of applying the non-splip condition in a range of situations. Nonetheless, recent discussions have demonstrated that fluid slippage can occur at the solid barrier, and that this criterion is not always met [37–41]. In fact, Navier [42] proposed the phenomenon

of frictional slippage at a stiff border approximately 200 years ago. Although the Stokesian movement equations under slip friction circumstances are of considerable importance for gases, slip conditions have recently been found to be significant for fluids as well, particularly when considering microscopic details. To estimate slip for fluids, Barrat et al. [43] made use of molecular dynamics. An excellent overview of experimental research on the slip phenomena of Newtonian fluid phases at a rigid surface was provided by Neto et al. [44]. The authors pay close attention to factors including wettability, surface roughness, and the presence of gaseous layers that influence fluid sliding at a rigid barrier. More attention has recently been paid to the application of the slip friction concept for Newtonian viscous fluid phases [45–51].

Recently, numerous articles have discussed several aspects of the flow of micropolar fluids using no-slip frictional circumstances for velocity and microrotation; examples in [52, 53]. In true situations, this boundary condition (no-slip) is not always satisfied. Often, there is sliding to some extent between the surfaces of the solid and the fluid. For the purpose of this study, we opted to discuss a micropolar movement problem where the velocity and microrotation present slip frictional circumstances. We propose a slip frictional framework for the microrotation based on the assumption that the component of the tangential couple stress at a given place on the fluid's surface is proportional to the component of tangential stress associated with the fluid's microrotation relative to the solid.

Numerous researchers [54, 55] have employed the slip-frictional phenomenon for the component of velocity but not for the microrotation. Since both microrotation and velocity occur at the same surface, applying the slip friction phenomenon to both components is more physically appropriate; its applicability is relevant due to the surface and fluid's properties. The axisymmetrical movement is inherently common in fluid dynamics as it naturally arises from the movement of any solid-fluid rotation.

The goal of this research is to determine the boundary effect on the quasi-steady movement of a micropolar fluid drop that is spheroidally shaped at a concentrical point within another immiscible viscous fluid in a spherical slip cavity. This paper extends the problem of Happel [56] to a micropolar fluid phase, allowing for the slipping condition for microrotation along with velocity. The problem is solved analytically and numerically. Also, at the droplet's surface, the spin-vorticity and microrotation relations are used.

2. Governing and constitutive equations

When body forces and couplings are absent, the governing equations for the slow, steady motion of a micropolar incompressible fluid, as mentioned by Eringen [32, 57], under the circumstances of low Reynolds numbers, are as follows:

$$\nabla \cdot \vec{u} = 0, \tag{2.1}$$

$$\nabla p = k\nabla \wedge \vec{v} + (\mu + k)\nabla \wedge \nabla \wedge \vec{u}, \tag{2.2}$$

$$k\nabla \wedge \vec{u} = 2k\vec{v} + \gamma\nabla \wedge \nabla \wedge \vec{v} - (\alpha + \beta + \gamma)\nabla\nabla \cdot \vec{v}, \tag{2.3}$$

where $\vec{u}$ represents the velocity vector; $\vec{v}$ represents the micro-rotation vector; and p is the fluid pressure. μ represents the dynamic viscosity coefficient. k represents the vortex viscosity coefficient.

Also, (α, β, γ) represent the gyro-viscosity coefficients. These constants follow the standard inequality formulas:

$$k \geq 0; \;\; 2\mu + k \geq 0; \;\; \gamma \geq 0; \;\; \gamma \geq |\beta|; \;\; 3\alpha + \beta + \gamma \geq 0.$$

The stress tensor equation, $\mathbf{\Pi}$, and the couple stress tensor equation, $\mathbf{m}$, are called the two constitutive equations:

$$\mathbf{\Pi} = -p\mathbf{I} + (2\mu + k)\triangle + k\boldsymbol{\varepsilon}\cdot(\vec{w} - \vec{v}), \tag{2.4}$$

$$\mathbf{m} = \alpha\mathbf{I} \cdot \nabla\vec{v} + \beta\nabla\vec{v} + \gamma\nabla^T\vec{v}, \tag{2.5}$$

here, $\mathbf{I}$ refers to the unit dyadic; $\boldsymbol{\varepsilon}$ refers to the alternating tensor, and $(\vec{w} = \frac{1}{2}\nabla \wedge \vec{q})$ represents the vorticity vector with $\triangle = \frac{1}{2}(\nabla\vec{q} + \nabla^T\vec{q})$ representing the deformation tensor rate; and $(\cdot)^T$ represents the transpose of a tensor.

3. Differential equations describe viscous and micropolar fluids

Refer to spherical coordinate systems by (r, θ, ϕ) with increasing directions and corresponding $(\vec{e}_r, \vec{e}_\theta, \vec{e}_\phi)$ unit vectors. For an arbitrary axisymmetric droplet translating steadily along the centre line of the motion, in a micropolar incompressible fluid, the velocity and microrotation vectors are of the form:

$$\vec{u} = u_r(r, \theta)\vec{e}_r + u_\theta(r, \theta)\vec{e}_\theta, \tag{3.1}$$

$$\vec{v} = v_\phi(r, \theta)\vec{e}_\phi. \tag{3.2}$$

From (2.1), we can write the velocity components with respect to the Stokesian stream function, ψ, as follows:

$$u_r = -\frac{1}{r^2 \sin\theta}\frac{\partial\psi}{\partial\theta}, \quad u_\theta = \frac{1}{r\sin\theta}\frac{\partial\psi}{\partial r}. \tag{3.3}$$

Substituting in the Eqs (2.2) and (2.3), we obtain

$$\frac{\partial p}{\partial r} + \left(\frac{\mu + k}{r^2\sin\theta}\right)\frac{\partial}{\partial\theta}[E^2\psi] - \left(\frac{k}{r\sin\theta}\right)\frac{\partial}{\partial\theta}[v_\phi \sin\theta] = 0, \tag{3.4}$$

$$\frac{\partial p}{\partial\theta} - \left(\frac{\mu + k}{\sin\theta}\right)\frac{\partial}{\partial r}[E^2\psi] + k\frac{\partial}{\partial r}[rv_\phi] = 0, \tag{3.5}$$

$$\gamma\,[E^2 v_\phi] + \left(\frac{k}{r\sin\theta}\right)[E^2\psi] - 2k[v_\phi] = 0, \tag{3.6}$$

where the axially symmetric Stokesian operator, E^2, is defined by

$$E^2 = \frac{\partial^2}{\partial r^2} + \frac{1 - \zeta^2}{r^2}\frac{\partial^2}{\partial\zeta^2}, \quad \zeta = \cos\theta.$$

In the absence of the microrotation v and the pressure p from Eqs (3.4)–(3.6), we obtain

$$E^4(E^2 - \ell^2)\psi = 0, \tag{3.7}$$

$$\nu = \frac{1}{2r\sin\theta}(E^2\psi + \frac{2\mu + k}{\ell^2 k}E^4\psi), \tag{3.8}$$

where $\ell^2 = a^2(2\mu + k)k/(\mu + k)\gamma$.

Consider that $\psi = \psi_1 + \psi_2$,
where

$$E^4\psi_1 = 0, \tag{3.9}$$
$$(E^2 - \ell^2)\psi_2 = 0. \tag{3.10}$$

Using the separation of variables, the general solutions of the Eqs (3.9) and (3.10) are:

$$\psi_1 = \sum_{n=2}^{\infty}(A_n r^n + B_n r^{2+n} + C_n r^{1-n} + D_n r^{3-n})G_n(\zeta), \tag{3.11}$$

$$\psi_2 = \sum_{n=2}^{\infty}\sqrt{r}(E_n I_{n-\frac{1}{2}}(\ell r) + F_n K_{n-\frac{1}{2}}(\ell r))G_n(\zeta), \tag{3.12}$$

where $I_n(\cdot)$ represents the modified Bessel function of order, n, of the first kind; $K_n(\cdot)$ represents the modified Bessel function of order, n, of the second kind; $G_n(\cdot)$ represents the Gegenbauer polynomial of the first kind of order, n, and degree $-\frac{1}{2}$; $[A_n, B_n, C_n, D_n, E_n, F_n, n \geq 2]$ are unknown constants.

4. Description and formulation of concentric spheres geometrically and analytically

In this section, we consider that the quasi-steady, slow flow of a nondeformable drop at the moment it passes the cavity's center is of great importance to discuss the slip cavity effects on a single droplet. Cunningham [58] has given an early analysis of Newtonian fluids for the slow-steady quasi-steady movement of a spherical rigid particle in a concentric cavity filled by Newtonian fluid. A similar solution was provided by Haberman et al. [59]. In both instances, the external cavity shape is supposed to be stiff, and a fluid sticks to it.

Assume a quasi-steady, slow flow generated by the movement of a drop of micropolar fluid, with radius a, that is spheroidally shaped at a concentrical point within another immiscible viscous fluid inside a spherical slip cavity, with radius $b(b > a)$. This drop sphere is moving with a constant velocity, $(\vec{U} = U\vec{e}_z)$, at a concentrical point, which is at rest, as demonstrated in Figure 1. Internal and external motions should be distinguished from one another. Suppose that $\psi^{(2)}$ represents the stream function of the micropolar flow in the drop, $(r \leq a)$, and $\psi^{(1)}$ represents the stream function for the viscous flow inside the slip cavity and outside the drop, $(a \leq r \leq b)$. There is no miscibility between the two fluid phases. As a consequence, the differential equations below are satisfied by the two stream functions:

$$E^4(E^2 - \ell^2)\psi^{(2)} = 0, \quad r \leq a, \tag{4.1}$$
$$E^4\psi^{(1)} = 0, \quad a \leq r \leq b. \tag{4.2}$$

The boundary circumstances at the inner slip cavity's surface and at the boundary between the micropolar droplet and the viscous fluid in the slip cavity must be given in order to complete this model.

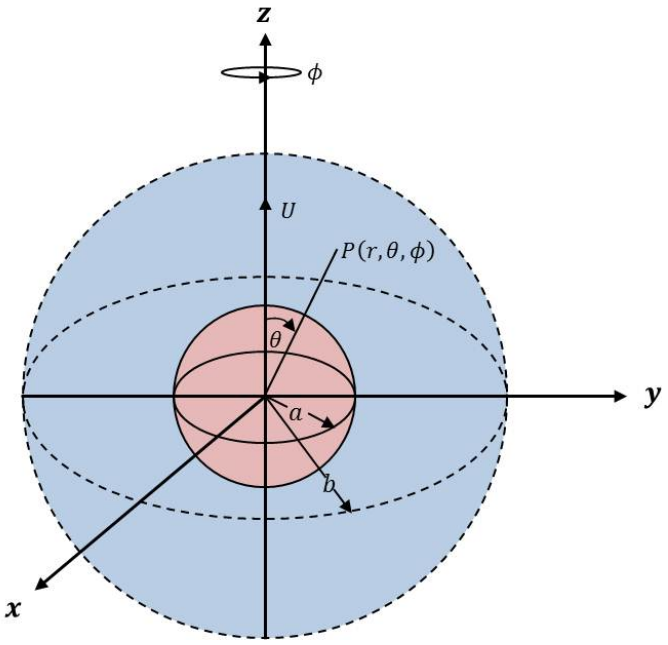

Figure 1. Sketching of a concentric sphere in geometric form.

4.1. At the droplet's surface ($r = a$)

At the interface, fluids both outside and inside the micropolar droplet are non-miscible, and the droplet's interface does not allow for mass transfer. As a result, the normal velocity component is zero on both sides of the drop. Furthermore, the component of tangential velocity is supposedly continuous across the interface. Assuming that the interfacial tension equilibrium theory applies to the current model, the interfacial tension only creates an interruption to the normal stress through the droplet's surface. Therefore, the tangential stress at the interface is not affected by interfacial tension; thus, the components of the tangential stress $(t_{r\theta}^{(1)}, t_{r\theta}^{(2)})$ must be continuous at the droplet's surface. Furthermore, under the aforementioned conditions, the component of microrotation of the micropolar fluid should be assigned as a boundary condition. Physically, in these circumstances, the most appropriate model is one in which the component of the vorticity for the viscous fluid outside the drop varies in direct proportion to the micropolar fluid's microrotation within it [60]. As a result, the spin coefficient between these two quantities is denoted by the parameter s; it varies from zero to one and simply relies on the nature of both fluid phases. There are two important conditions the microelements close to the droplet's surface are unable to rotate when $s = 0$, and the vorticity of the classical fluid is equal to the microrotation at the droplet's surface when $s = 1$. Also, the components of velocity must exist at the drop center. The following mathematical structure applies to the above-mentioned physical conditions:

$$u_r^{(1)} = u_r^{(2)} = U\cos\theta, \tag{4.3}$$

$$u_\theta^{(1)} = u_\theta^{(2)}, \tag{4.4}$$

$$t_{r\theta}^{(1)} = t_{r\theta}^{(2)}, \tag{4.5}$$

$$sw^{(1)} = v_\phi^{(2)}, \tag{4.6}$$

$$\lim_{r\to 0} u_r^{(2)}, \quad \lim_{r\to 0} u_\theta^{(2)}, \quad \lim_{r\to 0} v_\phi^{(2)}, \quad \text{exist.} \tag{4.7}$$

4.2. At the slip cavity's surface ($r = b$)

Owing to the slip cavity's impermeability, we assume

$$u_r^{(1)} = 0. \tag{4.8}$$

Assume the condition at the cavity's inner slip surface is as follows:

$$u_\theta^{(1)} = \tfrac{1}{\eta} t_{r\theta}^{(1)}, \tag{4.9}$$

where η is a slip frictional resistance. The rate of tangential slip between the imposed fluid and the inner wall of a rigid cavity is measured by the slip frictional resistance. Supposedly, the slip frictional resistance depends only on the characteristics of the imposed fluid and the inner rigid wall. There are two conditions; the first is a perfect slip at the cavity's internal surface when $\eta = 0$, in which case we have a spherical gas bubble inside the cavity, whereas the second is the no-slip condition, which is recovered when $\eta \to \infty$.

Using the differential equations (4.1) and (4.2) and the compliant boundary conditions, along with the support of the solutions (4.11) and (4.12), the appropriate solutions are given by

$$\psi^{(1)} = \tfrac{1}{2}(Ar^2 + Br^4 + Cr^{-1} + Dr)\sin^2\theta, \tag{4.10}$$

$$\psi^{(2)} = \tfrac{1}{2}(Mr^2 + Nr^4 + \sqrt{r}EI_{\frac{3}{2}}(\ell r))\sin^2\theta. \tag{4.11}$$

To satisfy the boundary conditions, the following hydrodynamical expressions must be used:

$$u_r^{(1)} = -(A + Br^2 + Cr^{-3} + Dr^{-1})\cos\theta, \tag{4.12}$$

$$u_\theta^{(1)} = \tfrac{1}{2}(2A + 4Br^2 - Cr^{-3} + Dr^{-1})\sin\theta, \tag{4.13}$$

$$w_\phi^{(1)} = \tfrac{1}{2}(2Ar^{-1} + 7Br + 2Cr^{-4} + Dr^{-2})\sin\theta, \tag{4.14}$$

$$t_{r\theta}^{(1)} = 3\mu_1(Br + Cr^{-4})\sin\theta, \tag{4.15}$$

$$u_r^{(2)} = -(M + Nr^2 + Er^{-\frac{3}{2}}I_{\frac{3}{2}}(\ell r))\cos\theta, \tag{4.16}$$

$$u_\theta^{(2)} = \left(M + 2Nr^2 - \tfrac{1}{2}Er^{-\frac{3}{2}}[I_{\frac{3}{2}}(\ell r) - \ell r I_{\frac{1}{2}}(\ell r)]\right)\sin\theta, \tag{4.17}$$

$$v_\phi^{(2)} = \tfrac{1}{2}(5Nr + m\ell^2 r^{-\frac{1}{2}}EI_{\frac{3}{2}}(\ell r))\sin\theta, \tag{4.18}$$

$$t_{r\theta}^{(2)} = \tfrac{1}{2}(2\mu_2 + k)\left(3Nr - Er^{-\frac{5}{2}}[\ell r I_{\frac{1}{2}}(\ell r) - 3I_{\frac{3}{2}}(\ell r)]\right)\sin\theta, \tag{4.19}$$

here, $m = [\mu_2 + k]/k$, μ_1 denotes the viscous fluid's viscosity coefficient, and μ_2 denotes the micropolar fluid's viscosity coefficient.

Using the expressions (4.12)–(4.19) along with the conditions (4.3)–(4.6), (4.8), and (4.9) to determine the seven unknown coefficients $[A, B, C, D, E, M, N]$, we derive the following system of linear equations:

$$Ab^3 + Bb^5 + C + Db^2 = 0, \tag{4.20}$$

$$A + Bb^2(2 - 3\delta_1^{-1}) - Cb^{-3}(\tfrac{1}{2} + 3\delta_1^{-1}) + \tfrac{1}{2}Db^{-1} = 0, \tag{4.21}$$

$$A + Ba^2 + Ca^{-3} + Da^{-1} - Ea^{-\frac{3}{2}} I_{\frac{3}{2}}(\ell a) - M - Na^2 = 0, \tag{4.22}$$

$$A + 2Ba^2 - \tfrac{1}{2}Ca^{-3} + \tfrac{1}{2}Da^{-1} + \tfrac{1}{2}Ea^{-\frac{3}{2}}(I_{\frac{3}{2}}(\ell a) - \ell a I_{\frac{1}{2}}(\ell a)) - M - 2Na^2 = 0, \tag{4.23}$$

$$A + Ba^2 + Ca^{-3} + Da^{-1} = -U, \tag{4.24}$$

$$3\lambda Ba + 3\lambda Ca^{-4} + Ea^{-\frac{5}{2}}(\ell a I_{\frac{1}{2}}(\ell a) - 3I_{\frac{3}{2}}(\ell a)) - 3Na = 0, \tag{4.25}$$

$$2sAa^{-1} + 7sBa + 2sCa^{-4} + sDa^{-2} - m\ell^2 a^{-\frac{1}{2}} E I_{\frac{3}{2}}(\ell a) - 5Na = 0, \tag{4.26}$$

where $\lambda = 2\mu_1/(2\mu_2 + k) = 2\mu/(2 + k/\mu_2)$, $\mu = \mu_1/\mu_2$ and $\delta_1 = b\eta/\mu_1$.

The drag force acting on a micropolar drop is given by [61]

$$W_z = 4\pi\mu D. \tag{4.27}$$

The above form (4.27) just relies on the unknown D and may be found using the Gaussian elimination method from the system solutions of the linear equations (4.20)–(4.26), which have a unique solution. We only need to record the value of D here, as follows:

$$D = Ua\frac{\Omega_1}{\Omega}, \tag{4.28}$$

where

$$\begin{aligned}\Omega_1 &= \tfrac{3}{2}(m\ell^2 a^2(1-\sigma^3) - \sigma_3)((2\lambda+3)\sigma_7\sigma^3 + 2\sigma_2(1+2\delta_1^{-1})) \\ &\quad + \tfrac{1}{2}\sigma_3\sigma_7(15\sigma^3 - 4s(1-\sigma^3)) - 3\sigma_3\sigma_5(1+2\delta_1^{-1}), \\ \Omega &= (m\ell^2 a^2(1-\sigma^3) - \sigma_3)(\sigma_2\sigma_6 - \sigma_1\sigma_7) + \sigma_3(\sigma_4\sigma_7 - \sigma_5\sigma_6),\end{aligned}$$

in which $\sigma = b/a$ and $\sigma_i, i = 1, 2, ..., 7$ are defined in the following form:

$$\sigma_1 = [\tfrac{3}{2}((1-\sigma^3) - 3(1-\sigma)\sigma^2) - 3(1-\sigma)\sigma^2\lambda], \tag{4.29}$$

$$\sigma_2 = [-\tfrac{3}{2}(2(1-\sigma^3) - 3(1-\sigma^2)\sigma^3) + 3(1-\sigma^5)\lambda], \tag{4.30}$$

$$\sigma_3 = \tfrac{5}{2}(1-\sigma^3)(\ell a\ell_1 - 3), \tag{4.31}$$

$$\sigma_4 = [\tfrac{15}{2}(1-\sigma)\sigma^2 - (\tfrac{5}{2} - s)(1-\sigma^3)], \tag{4.32}$$

$$\sigma_5 = [5(1-s)(1-\sigma^3) - \tfrac{15}{2}(1-\sigma^2)\sigma^3], \tag{4.33}$$

$$\sigma_6 = [(\sigma^{-1} - 2)(1-\sigma^3) + ((1+6\delta_1^{-1})\sigma^{-3} + 2)(1-\sigma)\sigma^2)], \tag{4.34}$$

$$\sigma_7 = [2((2-3\delta_1^{-1})\sigma^2 - 1)(1-\sigma^3) - ((1+6\delta_1^{-1})\sigma^{-3} + 2)(1-\sigma^2)\sigma^3)], \tag{4.35}$$

where $\ell_1 = \frac{I_{\frac{1}{2}}(\ell a)}{I_{\frac{3}{2}}(\ell a)}$.

For the purpose of comparison, the formula for the drag force W_∞ acting on a micropolar drop translating on an unbounded viscous fluid phase, is given by [10]

$$W_{z\infty} = -4\pi\mu_1 aU \times \frac{\ell^2 a^2(2\lambda + 3)(k+\mu_1)(\ell a + \Omega_2) + 15k\Omega_2(\lambda - 1)}{2\ell^2 a^2(\lambda + 1)(k+\mu_1)(\ell a + \Omega_2) - 5k\Omega_2(s - 3\lambda + 2)}, \tag{4.36}$$

where $\Omega_2 = \frac{3}{\tanh(\ell a)} - \frac{3}{\ell a} - \ell a$.

The correction wall factor $W = W_z/W_{z\infty}$, is given by:

$$W = -\frac{2\ell^2 a^2(\lambda + 1)(\mu_1 + k)(\ell a + \Omega_2) - 5k\Omega_2(s - 3\lambda + 2)}{\ell^2 a^2(2\lambda + 3)(\mu_1 + k)(\ell a + \Omega_2) + 15k\Omega_2(\lambda - 1)}\frac{\Omega_1}{\Omega}. \tag{4.37}$$

5. The no-slip frictional cavity case

Here, the condition (4.9), when slip frictional resistance is absent, has the following form:

$$u_\theta = 0, \qquad r = b. \tag{5.1}$$

Here, again, using (4.12)–(4.19) with the conditions (4.3)–(4.6), (4.8), and (5.1) to find the seven unknowns $[\hat{A}, \hat{B}, \hat{C}, \hat{D}, \hat{E}, \hat{M}, \hat{N}]$, we solve the following system:

$$\hat{A}b^3 + \hat{B}b^5 + \hat{C} + \hat{D}b^2 = 0, \tag{5.2}$$

$$\hat{A} + 2\hat{B}b^2 - \tfrac{1}{2}\hat{C}b^{-3} + \tfrac{1}{2}\hat{D}b^{-1} = 0, \tag{5.3}$$

$$\hat{A} + \hat{B}a^2 + \hat{C}a^{-3} + \hat{D}a^{-1} - \hat{E}a^{-\frac{3}{2}}I_{\frac{3}{2}}(\ell a) - \hat{M} - \hat{N}a^2 = 0, \tag{5.4}$$

$$\hat{A} + 2\hat{B}a^2 - \tfrac{1}{2}\hat{C}a^{-3} + \tfrac{1}{2}\hat{D}a^{-1} + \tfrac{1}{2}\hat{E}a^{-\frac{3}{2}}(I_{\frac{3}{2}}(\ell a) - \ell a I_{\frac{1}{2}}(\ell a)) - \hat{M} - 2\hat{N}a^2 = 0, \tag{5.5}$$

$$\hat{A} + \hat{B}a^2 + \hat{C}a^{-3} + \hat{D}a^{-1} = -U, \tag{5.6}$$

$$3\lambda\,\hat{B}a + 3\lambda\,\hat{C}a^{-4} - \hat{E}a^{-\frac{5}{2}}(\ell a I_{\frac{1}{2}}(\ell a) - 3I_{\frac{3}{2}}(\ell a)) - 3\hat{N}a = 0, \tag{5.7}$$

$$2s\hat{A}a^{-1} + 7s\hat{B}a + 2s\hat{C}a^{-4} + s\hat{D}a^{-2} - m\ell^2 a^{-\frac{1}{2}}\hat{E}I_{\frac{3}{2}}(\ell a) - 5\hat{N}a = 0. \tag{5.8}$$

Again, the drag force here just relies on the unknown $\hat{D}$, which is found using the Gaussian elimination method from the system solutions of the linear equations (5.2)–(5.8), which have a unique solution. We only need to record the value of $\hat{D}$ here, as follows:

$$\hat{D} = Ua\frac{\Omega_3}{\hat{\Omega}}, \tag{5.9}$$

where

$$\Omega_3 = \tfrac{3}{2}(m\ell^2a^2(1-\sigma^3) - \sigma_3)((2\lambda+3)\sigma^3\sigma_9 + 2\sigma_2) + \tfrac{1}{2}\sigma_3\sigma_9(15\sigma^3 - 4s(1-\sigma^3)) - 3\sigma_3\sigma_5,$$
$$\hat{\Omega} = m\ell^2a^2(1-\sigma^3)(\sigma_2\sigma_8 - \sigma_1\sigma_9) + \sigma_3(\sigma_4\sigma_9 - \sigma_5\sigma_8) - \sigma_3(\sigma_2\sigma_8 - \sigma_1\sigma_9),$$

in which σ_8 and σ_9 are defined in the following form:

$$\sigma_8 = [(\sigma^{-1} - 2)(1-\sigma^3) + (\sigma^{-3} + 2)(1-\sigma)\sigma^2], \tag{5.10}$$
$$\sigma_9 = [2(2\sigma^2 - 1)(1-\sigma^3) - (\sigma^{-3} + 2)(1-\sigma^2)\sigma^3]. \tag{5.11}$$

The correction wall factor $\hat{W}$ is given by:

$$\hat{W} = -\frac{2\ell^2a^2(\lambda+1)(\mu_1+k)(\ell a + \Omega_2) - 5k\Omega_2(s - 3\lambda + 2)}{\ell^2a^2(2\lambda+3)(\mu_1+k)(\ell a + \Omega_2) + 15k\Omega_2(\lambda-1)}\frac{\Omega_3}{\hat{\Omega}}. \tag{5.12}$$

Newtonian fluid's expression (5.12) is simplified to the following result recorded by Happel and Brenner [56]:

$$\bar{W} = \frac{\sigma[\sigma^5 - [\frac{1-\mu}{1+\frac{2}{3}\mu}]]}{\sigma^6 - \frac{9}{4}[\frac{1+\frac{2}{3}\mu}{1+\mu}]\sigma^5 + \frac{5}{2}[\frac{1}{1+\mu}]\sigma^3 - \frac{9}{4}[\frac{1-\frac{2}{3}\mu}{1+\mu}]\sigma + [\frac{1-\mu}{1+\mu}]}. \tag{5.13}$$

A few cases of (5.13):

(1) Solid sphere ($\mu \to 0$):

$$\bar{W} = \frac{\sigma(\sigma^5 - 1)}{\sigma^6 - \frac{9}{4}\sigma^5 + \frac{5}{2}\sigma^3 - \frac{9}{4}\sigma + 1}. \tag{5.14}$$

(2) Coalescence ($\mu = 1$):

$$\bar{W} = \frac{1}{\sigma^5 - \frac{15}{8}\sigma^4 + \frac{5}{4}\sigma^2 - \frac{3}{8}}. \tag{5.15}$$

(3) Gas bubble ($\mu \to \infty$):

$$\bar{W} = \frac{\sigma(\sigma^5 + \frac{3}{2})}{\sigma^6 - \frac{3}{2}\sigma^5 + \frac{3}{2}\sigma - 1}. \tag{5.16}$$

6. Discussion of the numerical results

The numerical findings of the two wall factors W and $\hat{W}$ appling to the nondeformable micropolar drop are shown in Figures 2–7 and Tables 1–4 for various parameters: The relative viscosity μ, the micropolarity parameter k/μ_1, the relative spacing a/b, the parameters ($\gamma/\mu_1 a^2$, δ_1).

As k, α, β, and γ are equal to zero, the issue is minimised by the movement of a viscous drop immersed in another viscous fluid phase. Moreover, Table 1 confirms that our numerical findings for the correction wall factor are in strong agreement with Happel's solutions [56].

Table 1. The correction wall factor that affects the Newtonian viscous droplet immersed in another viscous fluid phase.

	$\hat{W}$			$\bar{W}$ [56]		
a/b	$\mu \to 0$	$\mu = 1$	$\mu \to \infty$	$\mu \to 0$	$\mu = 1$	$\mu \to \infty$
0.1	1.28620	1.22891	1.17647	1.286	1.229	1.176
0.3	1.57264	2.12613	2.81519	2.573	2.126	1.815
0.5	7.29412	4.83019	3.72222	7.294	4.831	3.722
0.7	37.8296	18.7886	14.8255	37.830	18.762	14.826
0.9	1209.78	431.732	439.156	1209.778	431.779	439.156

Figure 2 shows that the correction factor $\hat{W}$ is increasing with the increase of a/b for several values of μ with $\gamma/\mu_1 a^2 = 0.3$, $s = 0.4$, and $k/\mu_1 \to 0$ with no-slip. Also, $\hat{W}$ decreases as the μ viscosity ratio increases, leaving the other parameters unaltered; if $a/b = 1$ is reached for each other parameter at any given value, it will eventually become limitless. As expected, Figure 2 displays that as $\mu \to 0$, a solid sphere case, $\hat{W}$ takes a larger value compared to a gas bubble case $\mu \to \infty$. Also, Table 2 confirms that the correction factor $\hat{W}$ decreases as μ increases; on the other hand, $\hat{W}$ increases as k/μ_1 increases.

Table 2. The correction wall factor $\hat{W}$ acting on a nondeformable drop for several values of μ, k/μ_1, a/b with $\gamma/\mu_1 a^2 = 0.2$ and $s = 0.3$.

		$\hat{W}$			
k/μ_1	a/b	$\mu = 0$	$\mu = 1$	$\mu = 10$	$\mu \to \infty$
0.000001	0.0	1.00000	1.00000	1.00000	1.00000
	0.1	1.28620	1.22891	1.18567	1.17647
	0.2	1.75584	1.57513	1.45299	1.42841
	0.3	2.57262	2.12618	1.86439	1.81519
	0.4	4.10587	3.06606	2.55698	2.46888
	0.5	7.29394	4.83032	3.87179	3.72222
	0.6	14.9476	8.63285	6.81464	6.56909
	0.7	37.8274	18.7891	15.1986	14.8255
	0.8	138.210	58.4127	51.0054	50.7734
	0.9	1209.52	431.739	430.354	439.156
	0.99	1317160	403018	472295	492642
5	0.0	1.02946	1.02630	1.01337	1.00000
	0.1	1.31603	1.29514	1.22756	1.17647
	0.2	1.78006	1.72007	1.54434	1.42841
	0.3	2.57337	2.42635	2.03896	1.81519
	0.4	4.03060	3.68141	2.87146	2.46888
	0.5	6.97729	6.12183	4.42647	3.72223
	0.6	13.7928	11.5107	7.79780	6.56910
	0.7	33.1046	25.9699	16.9743	14.8256
	0.8	110.752	80.6724	54.0087	50.7734
	0.9	800.997	545.952	421.482	439.155
	0.99	435115	382757	426290	492641
7	0.0	1.02838	1.02590	1.01451	1.00000
	0.1	1.31494	1.29789	1.23456	1.17647
	0.2	1.77917	1.72977	1.56216	1.42841
	0.3	2.57329	2.45136	2.07621	1.81519
	0.4	4.03311	3.74118	2.94366	2.46888
	0.5	7.98780	6.26547	4.56331	3.72223
	0.6	13.8299	11.8779	8.06103	6.56911
	0.7	33.2479	27.0381	17.5075	14.8256
	0.8	111.498	84.6662	55.1836	50.7734
	0.9	809.399	573.044	423.056	439.155
	0.99	4388325	384632	418233	492641

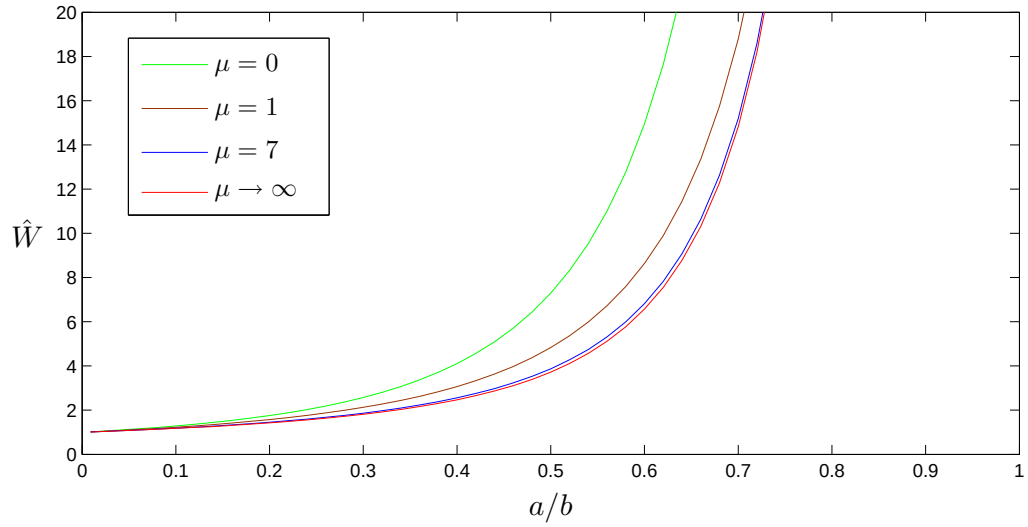

Figure 2. Plot of the correction wall factor $\hat{W}$ as opposed to the relative spacing a/b; for several values of μ, with $\gamma/\mu_1 a^2 = 0.3$, $s = 0.4$, and $k/\mu_1 \to 0$.

Figure 3 shows the correction wall factor W as opposed to the relative spacing a/b; for several values of the ratio δ_1 and μ. Predictably, W is increasing with the increase of a/b. Regarding any value that is specified of a/b, W increases with the increase of the ratio δ_1. Also, W increases along with the decrease of the ratio μ. Besides, Table 4 confirms that the correction factor W decreases as μ increases; on the other hand, W increases as the ratio δ_1 increases. As expected, Figure 3 and Table 4 show that the no-slip case $\delta_1 \to \infty$ gives us a greater value for W compared to the case of partial slip $\delta_1 \to 0$; therefore, the fluid sphere is affected by the presence of friction on the inner surface of the cavity.

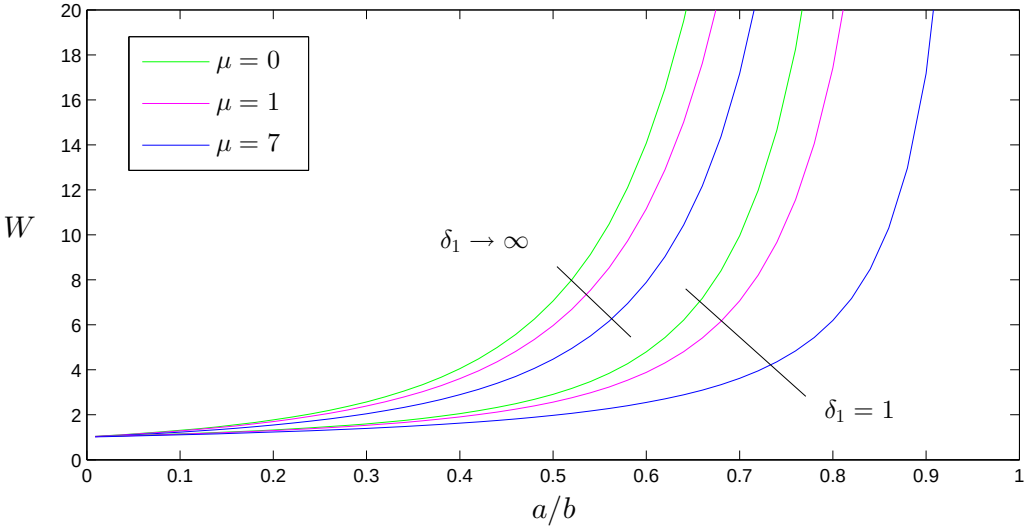

Figure 3. Plot of the correction wall factor W as opposed to the relative spacing a/b; for several values of δ_1 and μ with $k/\mu_1 = 3$, $s = 0.2$, and $\gamma/\mu_1 a^2 = 0.3$.

Figure 4 demonstrates the correction wall factor $\hat{W}$ when $\mu = 7$, and Figure 5 demonstrates the

correction wall factor W at $\mu = 7$ with the ratio $\delta_1 \to \infty$; both opposed to the ratio a/b; for different values of the ratio k/μ_1. The plots demonstrate that, the correction wall factors W and $\hat{W}$ are monotonically increasing along with the relative spacing a/b. $\hat{W}$ maintains approximately the same values when the micropolarity parameter increases; W is also the same. Thus, as expected, the wall correction factor is affected by the increase of the micropolarity parameter. Clearly, in the case of no slip $\delta_1 \to \infty$, Figure 5 matches Figure 4. In addition, the findings in Table 3 match those listed in Table 2.

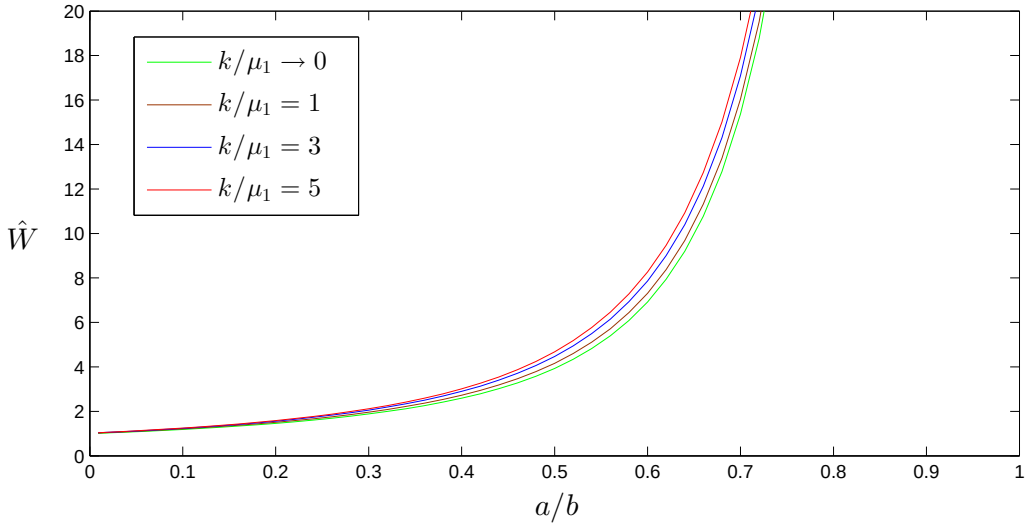

Figure 4. Plot of the correction wall factor $\hat{W}$ as opposed to the relative spacing a/b; for several values of the parameter k/μ_1 with $\gamma/\mu_1 a^2 = 0.3$, $s = 0.4$, and $\mu = 7$.

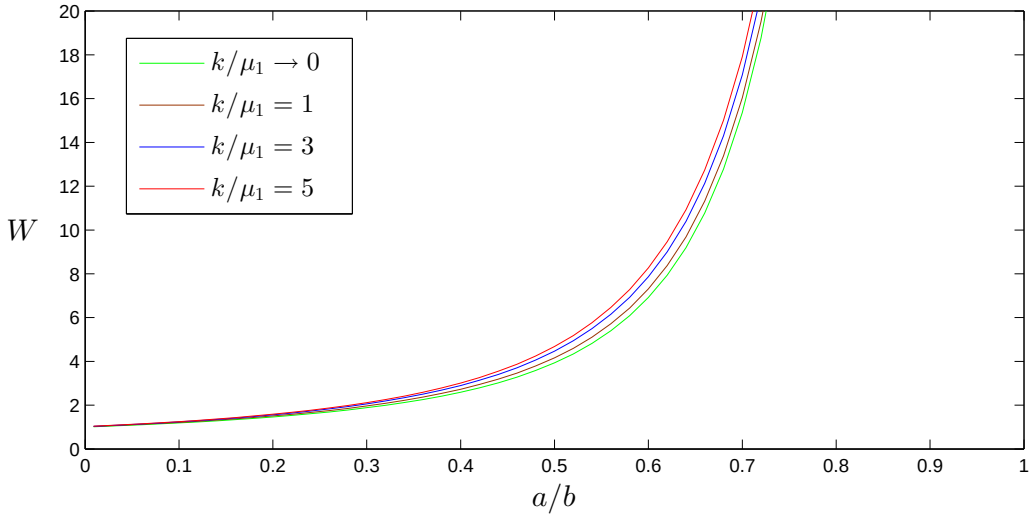

Figure 5. Plot of the correction wall factor W as opposed to the relative spacing a/b; for several values of k/μ_1 with $\delta_1 \to \infty$, $\gamma/\mu_1 a^2 = 0.3$, $s = 0.4$, and $\mu = 7$.

Table 3. The correction wall factor W acting on a nondeformable drop for several values of μ, k/μ_1, a/b with $\delta_1 \to \infty$, $\gamma/\mu_1 a^2 = 0.2$ and $s = 0.3$.

		W			
k/μ_1	a/b	$\mu = 0$	$\mu = 1$	$\mu = 10$	$\mu \to \infty$
0.000001	0.0	1.00000	1.00000	1.00000	1.00000
	0.1	1.28620	1.22891	1.18567	1.17647
	0.2	1.75584	1.57513	1.45299	1.42841
	0.3	2.57262	2.12618	1.86439	1.81519
	0.4	4.10587	3.06606	2.55698	2.46888
	0.5	7.29394	4.83032	3.87179	3.72222
	0.6	14.9476	8.63285	6.81464	6.56909
	0.7	37.8274	18.7891	15.1986	14.8255
	0.8	138.210	58.4127	51.0054	50.7734
	0.9	1209.52	431.739	430.354	439.156
	0.99	1317160	403018	472295	492642
5	0.0	1.02946	1.02630	1.01337	1.00000
	0.1	1.31603	1.29514	1.22756	1.17647
	0.2	1.78006	1.72007	1.54434	1.42841
	0.3	2.57337	2.42635	2.03896	1.81519
	0.4	4.03060	3.68141	2.87146	2.46888
	0.5	6.97729	6.12183	4.42647	3.72223
	0.6	13.7928	11.5107	7.79780	6.56910
	0.7	33.1046	25.9699	16.9743	14.8256
	0.8	110.752	80.6724	54.0087	50.7734
	0.9	800.997	545.952	421.482	439.155
	0.99	435115	382757	426290	492641
7	0.0	1.02838	1.02590	1.01451	1.00000
	0.1	1.31494	1.29789	1.23456	1.17647
	0.2	1.77917	1.72977	1.56216	1.42841
	0.3	2.57329	2.45136	2.07621	1.81519
	0.4	4.03311	3.74118	2.94366	2.46888
	0.5	7.98780	6.26547	4.56331	3.72223
	0.6	13.8299	11.8779	8.06103	6.56911
	0.7	33.2479	27.0381	17.5075	14.8256
	0.8	111.498	84.6662	55.1836	50.7734
	0.9	809.399	573.044	423.056	439.155
	0.99	4388325	384632	418233	492641

Table 4. The correction wall factor W acting on a nondeformable drop for several values of δ_1, a/b and μ with $\gamma/\mu_1 a^2 = 0.2$, $k/\mu_1 = 3$ and $s = 0.3$.

		W			
δ_1	a/b	$\mu = 0$	$\mu = 1$	$\mu = 10$	$\mu \to \infty$
0.1	0.0	1.02982	1.02554	1.01115	1.00000
	0.1	1.20343	1.18587	1.13816	1.10899
	0.2	1.44793	1.40606	1.30186	1.24464
	0.3	1.81545	1.72592	1.52082	1.41809
	0.4	2.41466	2.22418	1.82802	1.64771
	0.5	3.49950	3.07285	2.28748	1.96601
	0.6	6.76475	4.70431	3.04034	2.43653
	0.7	11.6031	8.45213	4.46283	3.20224
	0.8	33.0109	20.0681	7.93096	4.66425
	0.9	201.507	89.7226	23.2967	8.49491
100	0.0	1.02982	1.02554	1.01115	1.00000
	0.1	1.32010	1.29230	1.22020	1.17861
	0.2	1.79268	1.71301	1.52826	1.43474
	0.3	2.60611	2.41117	2.00955	1.83041
	0.4	4.11370	3.65147	2.82480	2.50521
	0.5	7.19977	6.06914	4.36955	3.81606
	0.6	14.4671	11.4510	7.80423	6.85247
	0.7	35.6739	26.1920	17.5550	15.9435
	0.8	126.079	85.0476	60.0498	58.0596
	0.9	1099.46	696.135	582.582	611.145
∞	0.0	1.02982	1.02554	1.01115	1.00000
	0.1	1.31639	1.28894	1.21766	1.17647
	0.2	1.78036	1.70221	1.52059	1.42841
	0.3	2.57340	2.38359	1.99101	1.81519
	0.4	4.02977	3.58385	2.78118	2.46888
	0.5	6.97385	5.89631	4.26027	3.72223
	0.6	13.7806	10.9563	7.48861	6.56910
	0.7	33.0579	24.4285	16.3757	14.8255
	0.8	110.510	75.2331	52.8055	50.7734
	0.9	798.293	512.093	421.466	439.156

Figures 6 and 7 show the correction wall factors $\hat{W}$ and W as opposed to the relative viscosity μ for several parameters. For the range ($0 \leq s \leq 1$), $\hat{W}$ and W decrease as the coefficient μ increases, maintaining the other coefficients unchanged. For every value of the coefficient μ stated, $\hat{W}$ and W increase as the parameter s decreases. This means that for $s = 1$, the microelements of the viscous fluid phase surrounding a micropolar drop are in perfect spin and $\hat{W}$ and W have their minimum; for $s = 0$, they have their maximum. Evidently, with values of the coefficient μ, the correction factor is irrelevant in terms of the spin coefficient. Further, $\hat{W}$ and W increase with the increase of the coefficient k/μ_1.

There are several solutions of the correction factor W for various values of the coefficients δ_1 and a/b, which are discussed in Table 4. Predictably, the findings in Table 4 demonstrate that the correction factor W with slippage is increasing with the relative spacing a/b for any value of the parameter δ_1. Generally speaking, the correction wall factor increases along with the parameter δ_1, holding a/b unaltered.

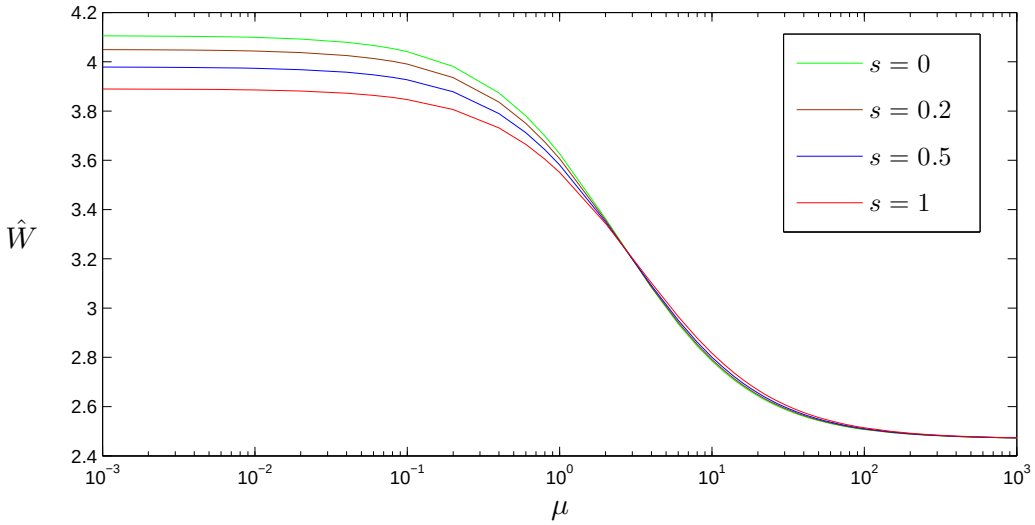

Figure 6. Plot of the correction wall factor $\hat{W}$ as opposed to the relative viscosity μ; for several values of s with $k/\mu_1 = 3$, $\gamma/\mu_1 a^2 = 0.3$, and $a/b = 0.4$.

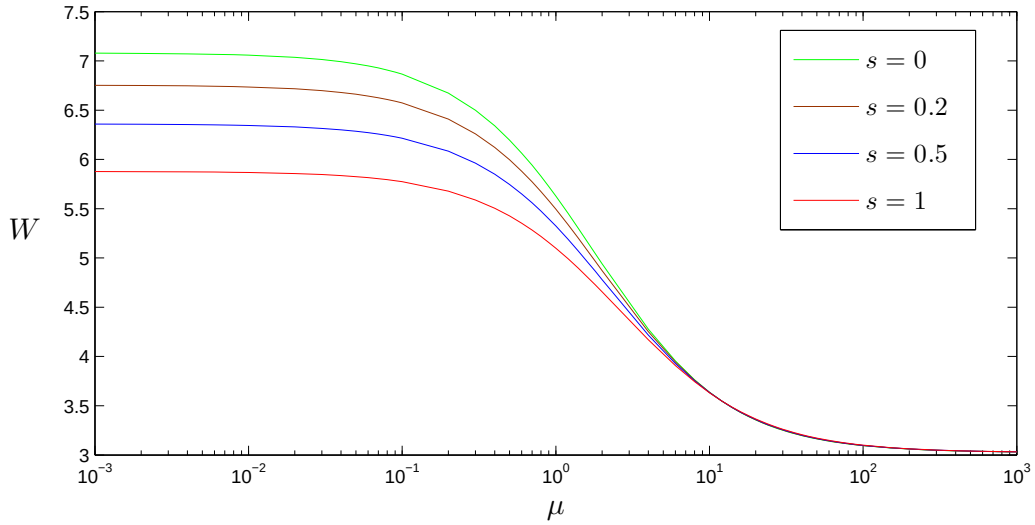

Figure 7. Plot of the correction wall factor W as opposed to the relative viscosity ratio μ; for several values of s with $k/\mu_1 = 3$, $\delta_1 = 5$, $\gamma/\mu_1 a^2 = 0.4$, and $a/b = 0.3$.

7. Conclusions

This research studies the axisymmetric movement of a micropolar fluid drop that is spheroidally shaped at a concentrical point within another immiscible viscous fluid inside a spherical slip cavity. At the droplet's surface, the vorticity-microrotation condition is applied. To find solutions to the Navier-Stokes equations both internal and external to the spherical droplet, spherical coordinate systems are used to find general solutions for velocity fields based on the concentric point within the cavity. This study expands on the issue addressed by Happel [56] to contain the effect of slip friction. Our findings agree with those by Happel [56]. Moreover, this study aims to determine the nondeformable droplet's response to the boundary. Finding expressions for the correction factors allows us to express the impact of droplet and cavity interactions. Clearly, as the gap thickness between the cavity and the droplet reaches zero, there is a strong interaction between them. These findings show that the correction wall factor takes a large value in the solid sphere case compared with the gas bubble case and in the no-slip case compared with the partial slip case. Also, it increases with the increase of the micropolarity parameter, takes a large value in the no-spin case compared with the perfect spin case, and decreases as the relative viscosity increases.

Use of AI tools declaration

The authors declare they have not used Artificial Intelligence (AI) tools in the creation of this article.

Conflict of interest

The authors declare that they have no known competing financial interests or personal relationships that could have appeared to influence the work reported in this paper.

References

1. S. S. Sadhal, P. S. Ayyaswamy, J. N. Chung, *Transport phenomena with drops and bubbles*, Springer Science & Business Media, 2012. https://doi.org/10.1007/978-1-4612-4022-8
2. U. Ali, K. U. Rehman, A. S. Alshomrani, M. Y. Malik, Thermal and concentration aspects in Carreau viscosity model via wedge, *Case Stud. Therm. Eng.,* **12** (2018), 126–133. https://doi.org/10.1016/j.csite.2018.04.007
3. M. Waqas, Z. Asghar, W. A. Khan, Thermo-solutal Robin conditions significance in thermally radiative nanofluid under stratification and magnetohydrodynamics, *Eur. Phys. J. Spec. Top.,* **230** (2021), 1307–1316. https://doi.org/10.1140/epjs/s11734-021-00044-w
4. K. U. Rehman, W. Shatanawi, Q. M. Al-Mdallal, A comparative remark on heat transfer in thermally stratified MHD Jeffrey fluid flow with thermal radiations subject to cylindrical/plane surfaces, *Case Stud. Therm. Eng.,* **32** (2022), 101913. https://doi.org/10.1016/j.csite.2022.101913
5. T. Kebede, E. Haile, G. Awgichew, T. Walelign, Heat and mass transfer in unsteady boundary layer flow of Williamson nanofluids, *J. Appl. Math.,* **2020** (2020), 1–13. https://doi.org/10.1155/2020/1890972

6. T. Walelign, E. Haile, T. Kebede, G. Awgichew, Heat and mass transfer in stagnation point flow of Maxwell nanofluid towards a vertical stretching sheet with effect of induced magnetic field, *Math. Probl. Eng.,* **2021** (2021), 1–15. https://doi.org/10.1155/2021/6610099
7. G. G. Stokes, On the effect of the internal friction of fluids on the motion of pendulums, *T. Cambridge Philos. Soc.,* **3** (1851), 8–106.
8. W. Rybczynski, Über die fortschreitende Bewegung einer flussigen Kugel in einem zahen Medium, *Bull. Acad. Sci. Cracovie A,* **1** (1911), 40–46.
9. M. J. Hadamard, Mécanique-mouvement permanent lent d'une sphèere liquide et visqueuse dans un liquid visqueux, *Compt. Rend. Acad. Sci.,* **152** (1911), 1735–1738.
10. R. Niefer, P. N. Kaloni, On the motion of a micropolar fluid drop in a viscous fluid, *J. Eng. Math.,* **14** (1980), 107–116. https://doi.org/10.1007/BF00037621
11. T. D. Taylor, A. Acrivos, On the deformation and drag of a falling viscous drop at low Reynolds number, *J. Fluid Mech.,* **18** (1964), 466–476. https://doi.org/10.1017/S0022112064000349
12. E. Bart, The slow unsteady settling of a fluid sphere toward a flat fluid interface, *Chem. Eng. Sci.,* **23** (1968), 193–210. https://doi.org/10.1016/0009-2509(86)85144-2
13. G. Hetsroni, S. Haber, E. Wacholder, The flow fields in and around a droplet moving axially within a tube, *J. Fluid Mech.,* **41** (1970), 689–705. https://doi.org/10.1017/S0022112070000848
14. H. Brenner, Pressure drop due to the motion of neutrally buoyant particles in duct flows. II. Spherical droplets and bubbles, *Ind. Eng. Chem. Fund.,* **10** (1971), 537–543. https://doi.org/10.1021/i160040a001
15. E. Wacholder, D. Weihs, Slow motion of a fluid sphere in the vicinity of another sphere or a plane boundary, *Chem. Eng. Sci.,* **27** (1972), 1817–1828. https://doi.org/10.1016/0009-2509(72)85043-7
16. E. Rushton, G. A. Davies, The slow unsteady settling of two fluid spheres along their line of centres, *Appl. Sci. Res.,* **28** (1973), 37–61. https://doi.org/10.1007/BF00413056
17. M. Coutanceau, P. Thizon, Wall effect on the bubble behaviour in highly viscous liquids, *J. Fluid Mech.,* **107** (1981), 339–373. https://doi.org/10.1017/S0022112081001808
18. M. Shapira, S. Haber, Low Reynolds number motion of a droplet between two parallel plates, *Int. J. Multiphase Flow,* **14** (1988), 483–506. https://doi.org/10.1016/0301-9322(88)90024-9
19. H. J. Keh, Y. K. Tseng, Slow motion of multiple droplets in arbitrary three-dimensional configurations, *AICHE J.,* **38** (1992), 1881–1904. https://doi.org/10.1002/aic.690381205
20. H. J. Keh, P. Y. Chen, Slow motion of a droplet between two parallel plane walls, *Chem. Eng. Sci.,* **56** (2001), 6863–6871. https://doi.org/10.1016/S0009-2509(01)00323-2
21. J. Magnaudet, S. H. U. Takagi, L. Dominique, Drag, deformation and lateral migration of a buoyant drop moving near a wall, *J. Fluid Mech.,* **476** (2003), 115–157. https://doi.org/10.1017/S0022112002002902
22. A. Z. Zinchenko, R. H. Davis, A multipole-accelerated algorithm for close interaction of slightly deformable drops, *J. Comput. Phys.,* **207** (2005), 695–735. https://doi.org/10.1016/j.jcp.2005.01.026

23. H. J. Keh, Y. C. Chang, Creeping motion of a slip spherical particle in a circular cylindrical pore, *Int. J. Multiphase Flow,* **33** (2007), 726–741. https://doi.org/10.1016/j.ijmultiphaseflow.2006.12.008
24. C. Pozrikidis, Interception of two spherical drops in linear Stokes flow, *J. Eng. Math.,* **66** (2010), 353–379. https://doi.org/10.1007/s10665-009-9301-3
25. K. Sugiyama, F. Takemura, On the lateral migration of a slightly deformed bubble rising near a vertical plane wall, *J. Fluid Mech.,* **662** (2010), 209–231. https://doi.org/10.1017/S0022112010003149
26. K. Sangtae, S. J. Karrila, *Microhydrodynamics: Principles and selected applications*, Courier Corporation, 2013.
27. T. C. Lee, H. J. Keh, Creeping motion of a fluid drop inside a spherical cavity, *Eur. J. Mech. B-Fluid.,* **34** (2012), 97–104. https://doi.org/10.1016/j.euromechflu.2012.01.008
28. K. U. Rehman, A. S. Alshomrani, M. Y. Malik, Carreau fluid flow in a thermally stratified medium with heat generation/absorption effects, *Case Stud. Therm. Eng.,* **12** (2018), 16–25. https://doi.org/10.1016/j.csite.2018.03.001
29. Z. Asghar, M. W. S. Khan, M. A. Gondal, A. Ghaffari, Channel flow of non-Newtonian fluid due to peristalsis under external electric and magnetic field, *Proc. I. Mech. Eng. Part E,* **236** (2022), 2670–2678. https://doi.org/10.1177/09544089221097693
30. A. G. Salem, M. S. Faltas, H. H. Sherief, Migration of nondeformable droplets in a circular tube filled with micropolar fluids, *Chinese J. Phys.,* **79** (2022), 287–305. https://doi.org/10.1016/j.cjph.2022.08.003
31. A. C. Eringen, Simple microfluids, *Int. J. Eng. Sci.,* **2** (1964), 205–217. https://doi.org/10.1016/0020-7225(64)90005-9
32. A. C. Eringen, Theory of micropolar fluids, *J. Math. Mech.,* 1966, 1–18. https://www.jstor.org/stable/24901466
33. V. K Stokes, *Theories of fluids with microstructure*, New York: Springer, 1984. https://doi.org/10.1007/978-3-642-82351-0_4
34. G. A. Graham, *Continuum mechanics and its applications*, Hemisphere Publishing Corporation, 1989, 707–720.
35. H. Hayakawa, Slow viscous flows in micropolar fluids, *Phys. Rev. E,* **61** (2000), 5477. https://doi.org/10.1103/PhysRevE.61.5477
36. T. Walelign, E. Seid, Mathematical model analysis for hydromagnetic flow of micropolar nanofluid with heat and mass transfer over inclined surface, *Int. J. Thermofluids,* **21** (2024), 100541. https://doi.org/10.1016/j.ijft.2023.100541
37. E. H. Kennard, *Kinetic theory of gases*, **483** (1938), New York: McGraw-hill. https://doi.org/10.1038/142494a0
38. D. K. Hutchins, M. H. Harper, R. L. Felder, Slip correction measurements for solid spherical particles by modulated dynamic light scattering, *Aerosol Sci. Tech.,* **22** (1995), 202–218. https://doi.org/10.1080/02786829408959741

39. P. A. Thompson, S. M. Troian, A general boundary condition for liquid flow at solid surfaces, *Nature,* **389** (1997), 360–362. https://doi.org/10.1038/38686
40. Z. Asghar, R. A. Shah, N. Ali, A computational approach to model gliding motion of an organism on a sticky slime layer over a solid substrate, *Biomech. Model. Mechan.,* **21** (2022), 1441–1455. https://doi.org/10.1007/s10237-022-01600-6
41. E. Seid, E. Haile, T. Walelign, Multiple slip, Soret and Dufour effects in fluid flow near a vertical stretching sheet in the presence of magnetic nanoparticles, *Int. J. Thermofluids,* **13** (2022), 100136. https://doi.org/10.1016/j.ijft.2022.100136
42. C. L. Navier, Mémoire sur les lois du mouvement des fluides, *Mem. Acad. Roy. Sci. I. Fr.,* **6** (1823), 389–440.
43. J. L. Barrat, Large slip effect at a nonwetting fluid-solid interface, *Phys. Rev. Lett.,* **82** (1999), 4671. https://doi.org/10.1103/PhysRevLett.82.4671
44. C. Neto, D. R. Evans, E. Bonaccurso, H. J. Butt, V. S. J. Craig, Boundary slip in Newtonian liquids: A review of experimental studies, *Rep. Prog. Phys.,* **68** (2005), 2859. https://doi.org/10.1088/0034-4885/68/12/R05
45. W. Jäger, A. Mikelić, On the roughness-induced effective boundary conditions for an incompressible viscous flow, *J. Differ. Equations,* **170** (2001), 96–122. https://doi.org/10.1006/jdeq.2000.3814
46. D. C. Tretheway, C. D. Meinhart, Apparent fluid slip at hydrophobic microchannel walls, *Phys. Fluids,* **14** (2002), L9–L12. https://doi.org/10.1063/1.1432696
47. G. Willmott, Dynamics of a sphere with inhomogeneous slip boundary conditions in Stokes flow, *Phys. Rev. E,* **77** (2008), 055302. https://doi.org/10.1103/PhysRevE.77.055302
48. D. Bucur, E. Feireisl, Š. Nečasová, Influence of wall roughness on the slip behaviour of viscous fluids, *P. Roy. Soc. Edinb. A,* **138** (2008), 957–973. https://doi.org/10.1017/S0308210507000376
49. F. Yang, Slip boundary condition for viscous flow over solid surfaces, *Chem. Eng. Commun.,* **197** (2009), 544–550. https://doi.org/10.1080/00986440903245948
50. H. Sun, C. Liu, The slip boundary condition in the dynamics of solid particles immersed in Stokesian flows, *Solid State Commun.,* **150** (2010), 990–1002. https://doi.org/10.1016/j.ssc.2010.01.017
51. H. Zhang, Z. Zhang, Y. Zheng, H. Ye, Corrected second-order slip boundary condition for fluid flows in nanochannels, *Phys. Rev. E,* **81** (2010), 066303. https://doi.org/10.1103/PhysRevE.81.066303
52. K. H. Hoffmann, D. Marx, N. D. Botkin, Drag on spheres in micropolar fluids with non-zero boundary conditions for microrotations, *J. Fluid Mech.,* **590** (2007), 319–330. https://doi.org/10.1017/S0022112007008099
53. A. G. Salem, Effects of a spherical slip cavity filled with micropolar fluid on a spherical viscous droplet, *Chinese J. Phys.,* **86** (2023), 98–114. https://doi.org/10.1016/j.cjph.2023.09.004
54. H. H. Sherif, M. S. Faltas, E. I. Saad, Slip at the surface of a sphere translating perpendicular to a plane wall in micropolar fluid, *Z. Angew. Math. Phys.,* **59** (2008), 293–312. https://doi.org/10.1007/s00033-007-6078-y

55. A. G. Salem, Effects of a spherical slip cavity filled with micropolar fluid on a spherical micropolar droplet, *Fluid Dyn. Res.,* **55** (2023), 065502. https://doi.org/10.1088/1873-7005/ad0ee3

56. J. Happel, H. Brenner, *Low Reynolds number hydrodynamics: With special applications to particulate media*, Germany: Springer Netherlands, 2012. https://doi.org/10.1007/978-94-009-8352-6

57. A. C. Eringen, *Microcontinuum field theories: II. Fluent media*, **2** (2001), Springer Science & Business Media.

58. E. Cunningham, On the velocity of steady fall of spherical particles through fluid medium, *Proc. Roy. Soc. London Ser. A,* **83** (1910), 357–365. https://doi.org/10.1098/rspa.1910.0024

59. W. L. Haberman, R. M. Sayre, *Motion of rigid and fluid spheres in stationary and moving liquids inside cylindrical tubes*, David Taylor Model Basin Washington DC, 1958. http://hdl.handle.net/1721.3/48988

60. N. P. Migun, On hydrodynamic boundary conditions for microstructural fluids, *Rheol. Acta,* **23** (1984), 575–581. https://doi.org/10.1007/BF01438797

61. H. Ramkissoon, S. R. Majumdar, Drag on an axially symmetric body in the Stokes' flow of micropolar fluid, *Phys. Fluids,* **19** (1976), 16–21. https://doi.org/10.1063/1.861320

AIMS Press